

## Edge-crack diagnosis using improved two-dimensional cracked finite element and micro genetic algorithm

Aysha Kalanad and B.N. Rao\*

*Structural Engineering Division, Department of Civil Engineering, Indian Institute of Technology Madras, Chennai 600 036, India*

In this paper, a crack diagnosis method based on an improved two-dimensional (2-D) finite element (FE) with an embedded edge crack, and micro genetic algorithm ( $\mu$ -GA) is proposed. The crack is not physically modelled within the element, but instead, its influence on the local flexibility of the structure is accounted for by the reduction of the element stiffness as a function of the crack length. The components of the stiffness matrix for the cracked element are determined from the Castigliano's first principle. The element was implemented in the commercial FE code ABAQUS as a user element subroutine. The accuracy of the proposed improved cracked element is verified by comparing the predicted first natural frequency with the available experimental data. Subsequently, a methodology to detect the crack location and size in conjunction with the proposed improved cracked element is formulated as an optimisation problem, and  $\mu$ -GA is used to find the optimal location and depth by minimising the cost function based on the difference of measured and calculated natural frequencies. The proposed crack detection procedure using the improved 2-D FE with an embedded edge crack, and  $\mu$ -GA is validated using the available experimental and FE modal analysis data reported in the existing literature. The predicted crack locations and crack sizes demonstrate that this approach is capable of detecting small crack location and depth with small errors.

**Keywords:** cracked finite element; micro genetic algorithm; user element; ABAQUS; natural frequency; crack diagnosis

### 1. Introduction

There is considerable interest in various damage detection methods for the quantitative diagnosis of structural crack through non-destructive testing. Quantitative diagnosis of cracks is an important part of predicting structural integrity and reliability of components, for a wide range of civil, mechanical and aeronautical engineering applications. Due to the practical importance of an early detection of cracks, the crack identification problem in structures has been extensively investigated and has led to the development of various methods. The presence of a crack in a structural member reduces the stiffness and increases the damping of the structure. As a consequence, there is a decrease in natural frequencies and modification of the modes of vibration. Therefore, it is possible to predict the location and the depth of a crack by measuring changes in the vibration parameters. The most useful damage localisation methods based on

---

\*Corresponding author. Email: [bnrao@iitm.ac.in](mailto:bnrao@iitm.ac.in)

vibration measurements are probably those based on examination of changes in natural frequencies, mode shapes or mode-shape curvatures. Changes in the natural frequencies are used more often than deviation of mode shapes, since frequencies can be measured more easily than mode shapes, and they are less seriously affected by experimental errors (Morassi, 2001). Many researchers have used the above characteristics to detect and locate cracks and a plethora of vibration-based methods for crack detection has been developed (Chaudhari & Maiti, 2000; Chinchalkar, 2001; Dado, 1997; Lee, 2009; Lele & Maiti, 2002; Liang, Choy, & Hu, 1991; Liang & Hu, 1993; Morassi, 2001; Nandwana & Maiti, 1997a, 1997b; Narkis, 1994; Nikolakopoulos, Katsareas, & Papadopoulos, 1997; Patil & Maiti, 2003; Rus, Lee, Chang, & Wooh, 2006; Rus, Lee, & Gallego, 2005; Shifrin & Ruotolo, 1999).

Reviews of research works dealing with the problem of crack detection based on changes in modal parameters can be found in the published literature (Doebbling, Farrar, Prime, & Shevitz, 1996; Montalvao, Maia, & Ribeiro, 2006; Salawu, 1997; Sohn et al., 2003). Messina, Williams, and Contursi (1998) presented a sensitivity and statistical-based method for structural damage detection. Kosmatka and Ricles (1999) proposed a modal vibration characterisation method using vibratory residual forces and weighted sensitivity analysis. Ratcliffe (2000) performed frequency and curvature-based experiments. Vestroni and Capecchi (2000) presented a method for concentrated damage detection based on natural frequency measurement. Gawronski and Sawicki (2000) adopted a method based on modal and sensor norms. Hu et al. (2001) presented a method using quadratic programming. Law, Chan, and Wu (2001) presented a method for large-scale structures using super-elements with the concept of damage detection orientation modelling. Sahin and Shenoii (2003) presented a damage detection algorithm using a combination of global and local vibration-based data as input to Artificial Neural Networks to predict the location and severity of the damage. Out of various vibration-based damage detection methods summarised, those based on updating structural model parameters can be reduced to the solution of constrained optimisation problems. Comparisons of the updated model parameters with the original correlated model parameters provide an indication of damage and can be used to quantify the location and the extent of the damage. However, for optimisation problems in which the objective function has many local maxima and minima, or when the variables are combinations of many discrete and continuous variables, it is difficult to use conventional optimisation algorithms such as the conjugate gradient method to obtain the global optimum.

In recent years, Genetic Algorithms (GAs) (Goldberg, 1989a, 1989b; Haupt & Haupt, 2004) have been recognised as promising intelligent search techniques for difficult optimization problems. GAs are search algorithms based on the mechanics of natural selection and natural genetics. They combine survival of the fittest among string structures with a structured yet randomised information exchange to form a search algorithm with some of the innovative flair of human search. While heuristic search methods such as simulated annealing or taboo search use one solution on their process to find the optimum point, GAs use the population of solutions to find the optimum point. It is known that with mathematical optimisation methods which use a gradient vector and Hessian, it is difficult to find the optimum point if there are a lot of local optima around the optimum point and a steep gradient around the optimum point (Goldberg, 1989a). GAs do not use a gradient vector and Hessian, but use object function value during their search. In its standard form, application of a GA requires the representation of design variables in terms of bit strings that are counterparts of

natural chromosomes, made up of a string of genes. GAs have actually found their applications in structural damage identification (Chou & Ghaboussi, 2001; Friswell, Penny, & Garvey, 1998; Harrison & Butler, 2001; Mares & Surace, 1996; Xia & Hao, 2001). Mares and Surace (1996) adopted GA to identify damage in elastic structures by defining a modified version of residual force vectors in terms of the stiffness matrix of the damaged structure as an objective function to be minimised while choosing stiffness reduction factors of all the elements as variables. However, this damage detection procedure is time consuming as the number of variables is equal to that of the elements in the finite element (FE) model. Krawczuk (2002) presented the wave propagation approach combined with GA for damage detection in beam-like structures. Sahoo and Maity (2007) trained a neural network (NN) considering the frequency and strain as the input parameters and the location and amount of the damage as the output parameters. They used a GA to select the NN parameters. The number of total runs, the number of GA generations, population size, and the NN training iterations are reported to be around 5, 100, 40, and 2000, respectively, so the number of mean square error evaluations is  $5 \times 100 \times 40 \times 2000 = 4 \times 10^7$  for a clamped free beam. However, their results are quite encouraging, but the NN training phase is very time consuming. Peimani, Vakil-Baghmisheh, Sadeghi, and Etefagh (2005) used multilayer perceptron networks for estimating the crack location.

It is recommended that more than 30 individuals should be used in GAs in order to prevent genetic drift (Mitchell, 1996). As the population size increases, chances of locating optimal solution increases and the GAs find a better solution. A bigger population size, however, requires more computational time to find the optimum solution (Goldberg, 1989a) and leads to slower convergence of the GA. For this reason, Goldberg (1989a, 1989b) proposed Serial Genetic Algorithms (SGAs) which use a small population size compared to conventional GAs. Based on SGAs, Krishnakumar (1989) proposed micro genetic algorithms ( $\mu$ -GAs).  $\mu$ -GAs use a relatively smaller population size than SGAs, resulting in less computational time. Moreover,  $\mu$ -GAs use elitism and convergence checking with reinitialisation to obtain the optimal or near optimal solutions.

To model the problem of a cracked beam using the FE method, several approaches have been used by various researchers. One-dimensional cracked beam FEs for vibration studies have been developed previously by other researchers (Chondros, Dimarogonas, & Yao 1998, 2001; Gounaris, Papadopoulos, & Dimarogonas, 1996; Krawczuk, Palacz, & Ostachowicz, 2003; Mahmoud, Abu Zaid, & Al Harashani, 1999; Papadopoulos & Dimarogonas, 1987). With an aim to simulate the crack presence without actually modelling the crack, more recently a two-dimensional (2-D) cracked FE was developed by Potirniche et al. (2008) for fatigue and fracture applications. In this approach, the influence of the additional flexibility of the element due to the crack presence was derived from the Castigliano's first theorem using fracture mechanics concepts. However, the accuracy of the predicted natural frequency using the cracked FE developed by Potirniche et al. (2008) for higher values of crack depth ratios is less. While deriving the components of the stiffness matrix for the cracked element Potirniche et al. (2008) assumed that the applied shear forces result only in mode II stress intensity factors (SIFs), and accordingly adopted the geometrical factor (for the effect of boundary conditions at free edge) corresponding to pure shear for infinite boundary conditions given in Tada, Paris, and Irwin (2000). It should be noted that the pure shear condition can be reproduced only when the shear force acting along an edge of the cracked element is accompanied by shear forces acting on three other faces.

However, when the applied shear force acts along an edge of the cracked element, as considered in Potirniche et al. (2008), mixed-mode conditions prevail, and not the pure shear condition, which results in both mode I and mode II SIFs. In addition, the adopted geometrical factor should take into account both the effect of finite size of the cracked element and the effect of boundary conditions at free edge.

This paper presents a crack diagnosis method based on an improved 2-D FE with an embedded edge crack, and  $\mu$ -GA. The crack is not physically modelled within the element, but instead, its influence on the local flexibility of the structure is accounted for by the reduction of the element stiffness as a function of the crack length. The components of the stiffness matrix for the cracked element are determined from the Castigliano's first principle. The element was implemented in the commercial FE code ABAQUS (2004) as a user element (UEL) subroutine. The accuracy of the UEL is verified by comparing the frequency response of various beams with an edge crack under bending. Later, a methodology to detect the crack location and size in conjunction with the proposed improved cracked element is formulated as an optimisation problem, and  $\mu$ -GA is used to find the optimal location and depth by minimising the cost function based on the difference of the measured and calculated natural frequencies. The organisation of the paper is as follows: Sections 2 and 3, respectively, present improved 2-D FE with an embedded edge crack and its validation. Section 4 outlines  $\mu$ -GA and  $\mu$ -GA-based crack identification procedure. Section 5 presents validation of  $\mu$ -GA-based crack identification technique using the available experimental and FE modal analysis data reported in the existing literature. Section 6 presents conclusions.

## 2. Improved cracked FE model

For predicting the natural frequency of a cracked beam more accurately, in this section, the following improvements to the cracked FE originally developed by Potirniche et al. (2008) are presented: (a) to handle crack depth ratios ranging up to .9; and (b) the additional flexibility of the cracked element due to the applied shear forces. Consider the cracked FE with the node numbering and the degrees of freedom per node as shown in Figure 1(a), the mathematical definition details of which are given in Potirniche et al. (2008).

In Figure 1(b), the tensile force at node 3 gives a force and a moment, both of which contribute to an opening of the crack. Hence, the contribution  $K_{IF_3}$  of the nodal force  $F_3$  at node 3 is summation of the SIFs given by the force and the resulting bending moment  $F_3 h/2$  ( $h$  is the element depth), which can be written as

$$K_{IF_3} = K_{IF_3}^f + K_{IF_3}^m, \quad (1)$$

where

$$K_{IF_3}^f = F_f \frac{F_3}{ht} \sqrt{\pi\alpha} \quad \text{and} \quad K_{IF_3}^m = F_m \frac{3F_3}{ht} \sqrt{\pi\alpha}, \quad (2)$$

with the geometrical factors  $F_f$  and  $F_m$  for the cracked element under tensile and bending loading, respectively, and  $t$  being the element thickness.

The FRANC2DL FE code (Gondhalekar, 1992; James and Swenson, 1999; Wawrzynek & Ingraffea, 1987, 1994) is used with the J-integral option to extract the SIFs from stress-strain fields around the crack tip location. 2-D, FE models having

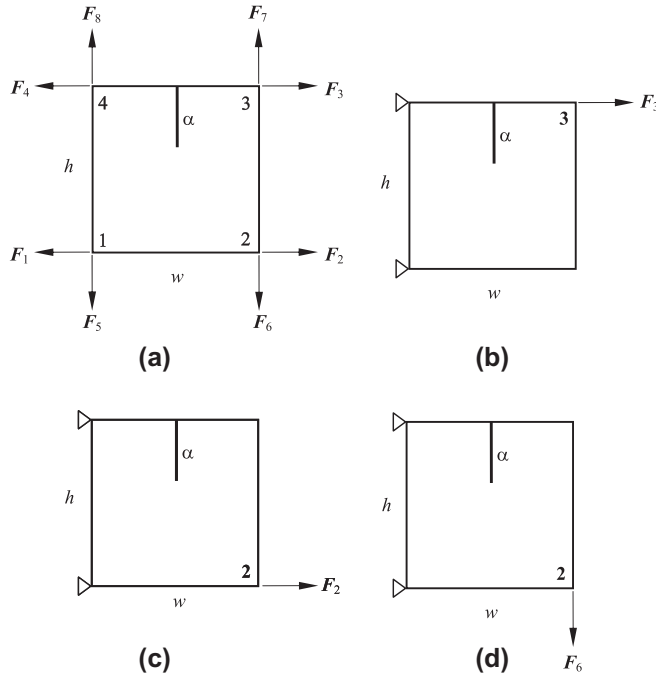


Figure 1. 2-D cracked FE; (a) Node numbering and degrees of freedom at all nodes; (b) Nodal force  $F_3$  at node 3; (c) Nodal force  $F_2$  at node 2; and (d) Nodal force  $F_6$  at node 2.

$w/h = 2$  with degrees of freedom ranging from 3510 (for the case  $\alpha/h = .1$ ) to 4258 (for the case  $\alpha/h = .9$ ), along with a ring of six-noded quarter-point elements around the crack tip and eight-noded elements elsewhere are used under plane stress conditions. The minimum element size at the crack tip location is  $.0025w$ . Crack length to depth ratios ( $\alpha/h$ ) are varied from  $.1$  to  $.9$  with nodal forces applied at various locations on the cracked element. Using the SIFs values obtained from FRANC2DL for  $\alpha/h$  ranging from  $.1$  to  $.9$ , and Equation 2, the geometrical factors  $F_f$  and  $F_m$  are obtained by curve fitting techniques as a function of  $\alpha/h$  as follows:

$$F_f\left(\frac{\alpha}{h}\right) = 2.6233 - 51.173\frac{\alpha}{h} + 551.45\left(\frac{\alpha}{h}\right)^2 - 2563.7\left(\frac{\alpha}{h}\right)^3 + 5883.6\left(\frac{\alpha}{h}\right)^4 - 6472.2\left(\frac{\alpha}{h}\right)^5 + 2750.4\left(\frac{\alpha}{h}\right)^6, \quad (3)$$

and,

$$F_m\left(\frac{\alpha}{h}\right) = 1.6426 - 18.687\frac{\alpha}{h} + 192.08\left(\frac{\alpha}{h}\right)^2 - 883.57\left(\frac{\alpha}{h}\right)^3 + 2018.3\left(\frac{\alpha}{h}\right)^4 - 2213.7\left(\frac{\alpha}{h}\right)^5 + 939\left(\frac{\alpha}{h}\right)^6. \quad (4)$$

The above given geometrical factors  $F_f$  and  $F_m$  are validated for other cases with  $w/h > 2.0$  by comparing the SIFs values obtained from FRANC2DL with those values obtained using Equation 2 in conjunction with Equations 3 and 4. The effect of  $w/h$  is found to be practically negligible for  $w/h \geq 2.0$ .

Contrary to the tensile force acting at node 3 (in Figure 1(b)) as discussed above, in Figure 1(c), the nodal force  $F_2$  acting at node 2 results in a force that leads to an opening of the crack and a resolved bending moment that leads to the closing of the crack. Hence, the contribution  $K_{IF_2}$  of the nodal force  $F_2$  at node 2 can be written as

$$K_{IF_2} = K_{IF_2}^f - K_{IF_2}^m, \tag{5}$$

where

$$K_{IF_2}^f = F_f \frac{F_2}{ht} \sqrt{\pi\alpha} \quad \text{and} \quad K_{IF_2}^m = F_m \frac{3F_2}{ht} \sqrt{\pi\alpha}, \tag{6}$$

with the geometrical factors  $F_f$  and  $F_m$  defined in Equations 3 and 4.

Following the procedure based on Castigliano's first theorem, outlined by Potirniche et al. (2008), the stiffness components  $K_{2j}$  and  $K_{3j}$  can be obtained using the geometrical factors  $F_f$  and  $F_m$  defined in Equations 3 and 4. The stiffness components  $K_{1j}$  and  $K_{4j}$  can also be obtained following the same procedure as that for the stiffness components  $K_{2j}$  and  $K_{3j}$ .

In Figure 1(d), the nodal force  $F_6$  acting at node 2 gives a shear force and a moment ( $Fw$ ), both of which contribute to mode I and II SIFs, which can be written as

$$K_{IF_6} = F_I \frac{6Fw}{h^2t} \sqrt{\pi\alpha} \quad \text{and} \quad K_{IIF_6} = F_{II} \frac{F}{ht} \sqrt{\pi\alpha}. \tag{7}$$

Using the SIFs values obtained from FRANC2DL for  $\alpha/h$  ranging from .1 to .9, and Equation 7, the geometrical factors for the cracked element  $F_I$  and  $F_{II}$ , respectively, are obtained by curve-fitting techniques as a function of  $\alpha/h$  as follows:

$$F_I \left( \frac{\alpha}{h} \right) = .821 - 9.344 \frac{\alpha}{h} + 96.04 \left( \frac{\alpha}{h} \right)^2 - 441.78 \left( \frac{\alpha}{h} \right)^3 + 1009.15 \left( \frac{\alpha}{h} \right)^4 - 1106.85 \left( \frac{\alpha}{h} \right)^5 + 469.5 \left( \frac{\alpha}{h} \right)^6, \tag{8}$$

and

$$F_{II} \left( \frac{\alpha}{h} \right) = 1.018 - 17.794 \frac{\alpha}{h} + 162.7 \left( \frac{\alpha}{h} \right)^2 + 596.45 \left( \frac{\alpha}{h} \right)^3 + 1098.3 \left( \frac{\alpha}{h} \right)^4 - 994.94 \left( \frac{\alpha}{h} \right)^5 + 353.26 \left( \frac{\alpha}{h} \right)^6. \tag{9}$$

The stiffness components  $K_{6j}$  can be obtained adopting the following procedure. Using Castigliano's first theorem, the difference between the nodal forces in the cracked ( $F_i$ ) and undamaged ( $F_i^0$ ) cases can be obtained by taking the partial derivatives of the SIFs with respect to the corresponding displacements ( $u_i$ ) by the relation (Tada et al., 2000),

$$F_6^0 - F_6 = \frac{2t}{E'} \left[ \int_0^\alpha K_I \frac{\partial K_I}{\partial u_6} da + \int_0^\alpha K_{II} \frac{\partial K_{II}}{\partial u_6} da \right] \tag{10}$$

where  $E' = E$  for plane stress,  $E' = E/(1 - \nu^2)$  for plane strain and  $E$  and  $\nu$  are the modulus of elasticity and Poisson's ratio, respectively. Replacing the SIFs in the above equation with their respective formulas in Equation 7 and after some simplifications, one obtains

$$F_6^0 - F_6 = \frac{2\pi}{E'h^2t} \left[ \frac{36w^2}{h^2} \int_0^z aF_I^2 da + \int_0^z aF_{II}^2 da \right] F_6 \frac{\partial F_6}{\partial u_6}. \quad (11)$$

Defining  $A_{66}$  as,

$$A_{66} = \frac{2\pi}{E'h^2t} \left[ \frac{36w^2}{h^2} \int_0^z aF_I^2 da + \int_0^z aF_{II}^2 da \right], \quad (12)$$

and noting that

$$\frac{\partial F_6}{\partial u_6} = K_{66}, \quad (13)$$

the relation between the two nodal forces for the undamaged and cracked elements becomes

$$F_6^0 = (1 + A_{66}K_{66})F_6. \quad (14)$$

Using  $\{F^0\} = [K^0]\{u\}$  which corresponds to the undamaged element, Equation 14 can be written as

$$\sum_{j=1}^8 K_{6j}^0 u_j = \sum_{j=1}^8 (1 + A_{66}K_{66})K_{6j} u_j, \quad (15)$$

which is valid only if the coefficients multiplying the independent variables  $u_j$  on both sides of the above equation are equal.

$$K_{6j}^0 = (1 + A_{66}K_{66})K_{6j} \quad \text{for } j = 1, 2, \dots, 8. \quad (16)$$

Solving Equation 16 for  $K_{6j}$ , the solution is found to be

$$K_{66} = \frac{-1 + \sqrt{1 + 4A_{66}K_{66}^0}}{2A_{66}}, \quad (17)$$

and

$$K_{6j} = \frac{2K_{6j}^0}{1 + \sqrt{1 + 4A_{66}K_{66}^0}} \quad \text{for } j = 1, 2, \dots, 8 \text{ and } j \neq 6. \quad (18)$$

Similar formulas can be obtained for all the components  $K_{5j}$ ,  $K_{7j}$  and  $K_{8j}$ .

### 3. Validation of cracked FE

The proposed improved 2-D FE with an embedded edge crack is implemented in the commercial FE code ABAQUS (2004) as a User Element Fortran subroutine (UEL.f). The performance of the proposed improved FE is demonstrated by comparing the frequency ratio ( $\omega_c/\omega$ ) (ratio of the natural frequency of the cracked beam to that of the uncracked beam) vs. the crack depth ratio ( $\alpha/H$ ) (the ratio of the crack depth ( $\alpha$ ) to the beam height ( $H$ )) results obtained using UEL, with the reported results in the literature, for the bending mode, for various crack location ratios ( $c/L$ ) (ratio of the crack location to the beam length). The following beam cases are considered: (1) simply supported beam with a double-edge surface crack at mid span; (2) cantilever beam with a surface crack at 20% of the beam span from fixed end; and (3) simply supported beam with a surface crack at mid span. In the numerical study, the crack depth ratio ( $\alpha/H$ ) is varied from 0 to .5.

#### 3.1. Simply supported beam with a double edge surface crack

In this numerical example, a steel beam (Chondros et al., 1998) having the length  $L = .575$  m, the height  $H = .03175$  m, the thickness  $t = .00952$  m with  $E = 2.06 \times 10^{11}$  N/m<sup>2</sup> and  $\rho = 7800$  kg/m<sup>3</sup> is considered. Figure 2 shows typical FEM discretisation with 36 standard four-node ABAQUS (2004) elements and one UEL each at the top and the bottom at the top of the beam for  $c/L = .5$ . Figure 3 shows the first natural frequency ratio ( $\omega_c/\omega$ ) vs. the crack depth ratio ( $\alpha/H$ ) for simply supported beam with two surface cracks, at the top and bottom edges of the beam at mid span.

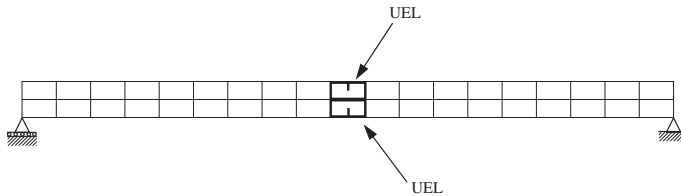


Figure 2. Discretisation of simply supported beam with double-edge surface crack using 36 standard four-node ABAQUS elements and two UELs.

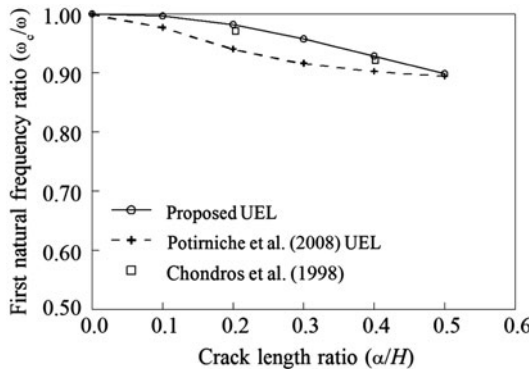


Figure 3. First natural frequency ratio vs. the crack depth ratio for simply supported beam with double-edge surface crack at mid span.

Compared with the predictions obtained using the damaged FE by Potirniche et al. (2008), the first natural frequency reduction predicted by the proposed improved 2-D FE matches very well with the experiments results by Chondros et al. (1998).

**3.2. Cantilever beam with a surface crack**

In this numerical example, a steel cantilever beam (Wendtland, 1972) with all the geometric and material properties same as that of simply supported beam with a double-edge surface crack, except having the height  $H = .0242m$ , is considered. Typical FEM discretisation with 22 standard four-node ABAQUS (2004) elements and one UEL for  $c/L = .2$  measured from fixed end is shown in Figure 4. Figure 5 shows the first natural frequency ratio ( $\omega_c/\omega$ ) vs. the crack depth ratio ( $\alpha/H$ ) for steel cantilever beam with crack located at a distance of 20% of the beam length from the fixed end. Compared with the predictions obtained using the damaged FE by Potirniche et al. (2008), the first natural frequency reduction predicted by the proposed improved 2-D FE matches very well with the experiments results (Wendtland, 1972). Contrary to the

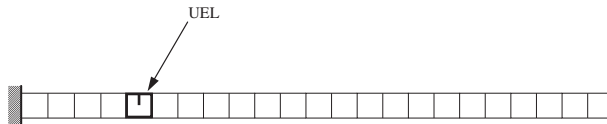


Figure 4. Discretisation of cantilever beam with surface crack using 22 standard four-node ABAQUS elements and one UEL.

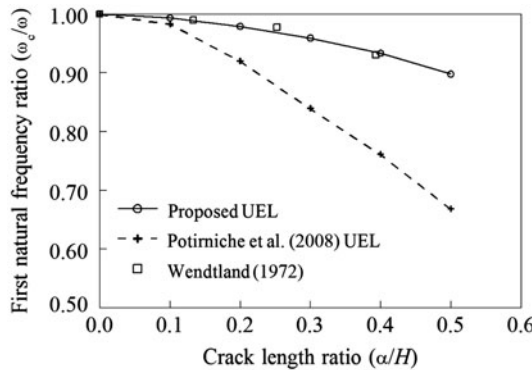


Figure 5. First natural frequency ratio vs. the crack depth ratio for cantilever beam with surface crack with crack at 20% of beam length from fixed end.

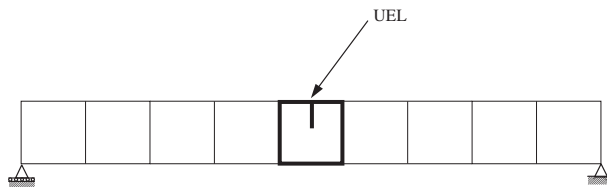


Figure 6. Discretisation of simply supported beam with surface crack using eight standard four-node ABAQUS elements and one UEL.

reported results (Potirniche et al., 2008), the current study showed much deviation in the predictions obtained using the damaged FE by Potirniche et al. (2008), when compared with the experimental results (Wendtland, 1972).

**3.3. Simply supported beam with a surface crack**

An aluminium beam (Chondros et al., 1998) having the length  $L = .235$  m, the height  $H = .0254$  m and the thickness  $t = .006$  m with the elastic modulus

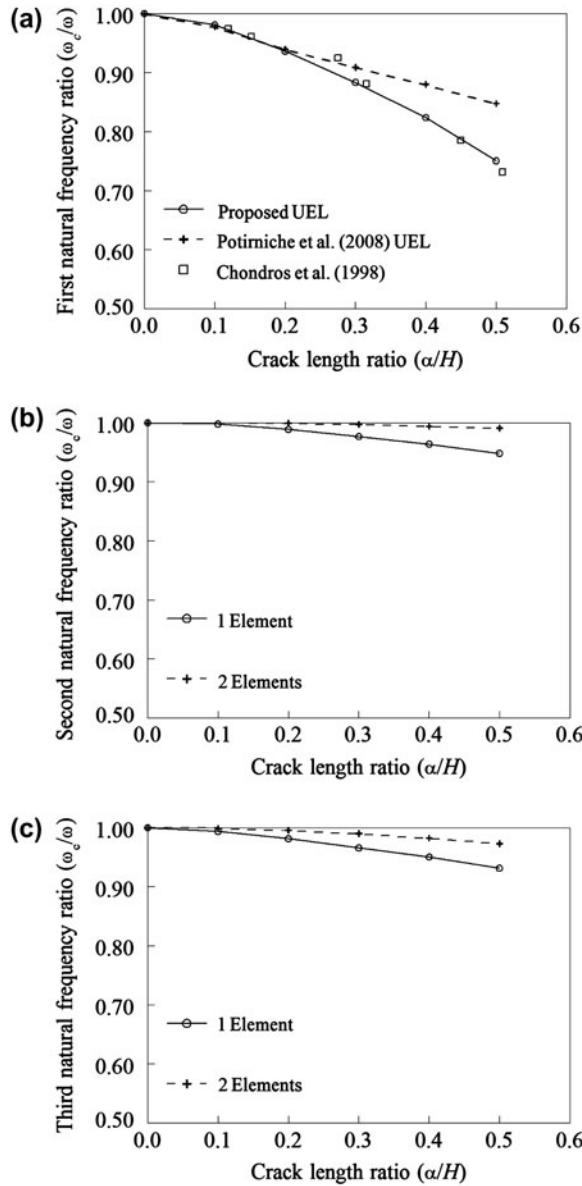


Figure 7. Variation in natural frequency reduction of simply supported beam with surface crack at mid span; (a) First mode with surface crack at mid span; (b) Second mode with surface crack at mid-span; and (c) Third mode with surface crack at  $c/L = 1/3$ .

$E = 7.2 \times 10^{10}$  N/m<sup>2</sup> and the density  $\rho = 2800$  kg/m<sup>3</sup>, is considered. Typical FEM discretisation with 8 standard four-node ABAQUS (2004) elements and one UEL for  $c/L = .5$  is shown in Figure 6. Figure 7(a) shows the first natural frequency ratio ( $\omega_c/\omega$ ) vs. the crack depth ratio ( $\alpha/H$ ) for simply supported beam with a surface crack at mid span. Compared with the predictions obtained using the damaged FE by Potirniche et al. (2008), the first natural frequency reduction predicted by the proposed improved 2-D FE matches very well with the experimental results by Chondros et al. (1998).

For the simply supported beam case considered above, FEM discretisation with the height of UEL equal to the beam height is adopted. In the following, the effect of the number of elements along the direction of the beam height on the accuracy in predicting the reduction in the natural frequencies of higher modes is studied.

Noting that if the crack location coincides with the vibration node of one of the modes, the frequency for that mode remains almost unchanged, Figure 7(b) shows variation in the natural frequency reduction of second mode of simply supported beam with a surface crack at mid span with respect to the number of elements along the direction of the beam height, predicted by the proposed improved 2-D FE for various values of the crack depth ratios ( $\alpha/H$ ). Similarly, Figure 7(c) shows the variation in the natural frequencies reduction of the third mode of simply supported beam with a surface crack at  $c/L = 1/3$  measured from the support, with respect to the number of elements along the direction of the beam height. It can be observed from Figures 7(b) and (c) that by adopting two elements along the direction of the beam height, better accuracy can be obtained in the prediction of reduction in the natural frequencies of higher modes, which are essential for predicting the crack location and size. Hence, in the crack identification technique presented in the subsequent sections, two elements along the direction of the beam height are adopted and when the crack depth is equal to the height of UEL, the element stiffness is assumed to be zero.

#### 4. Crack identification technique

The improved 2-D FE with an embedded edge crack is implemented in the commercial FE code ABAQUS (2004) as a UEL.f to evaluate the natural frequencies.

##### 4.1. Micro genetic algorithm

To estimate the location and depth of a crack in a structure using natural frequency information, GA is adopted. The inputs to the proposed crack detection system are the natural frequency ratios ( $\omega_c/\omega$ ) (ratio of the natural frequency of the cracked beam to that of the uncracked beam). The identification of the crack location and depth is formulated as an optimisation problem that is solved to find the optimal crack location and depth by minimising the objective/fitness function which is based on the difference of measured and calculated frequencies. Conventional optimisation techniques have difficulty in finding the global minimum unless the starting point is in the immediate vicinity of it. GAs and  $\mu$ -GAs are popular methods for global search (Goldberg, 1989a, 1989b; Krishnakumar, 1989). The constrained optimisation problem is typically converted into an unconstrained problem by penalising vectors that violate constraints (Osyczka & Kundu, 1996; Pezeshk, Camp, & Chen, 2000). The efficiency of the conventional optimisation techniques can be further improved by adopting the qualitative construction of a reliable initial guesses within non-iterative computational

frameworks (Amstutz, Horchani, & Masmoudi, 2005; Cakoni & Colton, 2003; Garreau, Guillaume, & Masmoudi, 2000).

In the present study, the  $\mu$ -GA based on Carroll's work (Carroll, 1996) is adopted with tournament selection, uniform crossover and an elitism scheme. The GA driver initialises a random sample of individual solutions upon the initiation of the algorithm. Binary encoding is adopted for individual solutions in the population. Carroll (1996) and Lee, Kim, Park, and Woo (2005) suggested using  $\mu$ -GAs with a population size of 5 or 10. In the present study, the  $\mu$ -GAs with the various population sizes of 5, 8, 10, 12 and 15 individuals are examined and similar convergence histories are observed. A *tournament selection* method is used to select parent genes on which the *uniform crossover* operation (that replaces the discarded chromosomes in a population by new chromosomes) is applied with a crossover rate of 1.0. One important attribute of uniform crossover is that this technique tends to preserve variety in the genetic group. In the  $\mu$ -GA, there are two convergence criteria called inner and outer criteria. Due to the lack of adequate diversity in the small population, it is unlikely that the process converges into a true value in the inner loop operations. In the inner loop, if the entire population is converged to a nominal value with the other individuals being sufficiently similar to the best individual solution in the population (with less than a total of 5% difference), then the process goes out of the inner loop (Carroll, 1996). The outer loop is performed until the total number of generations reaches a prescribed value. Therefore, the number of inner loops varies from generation to generation, but the total number of generations is fixed. In order to prevent the possibility of losing good genes, an *elitism* scheme (that makes a copy of the best chromosomes of a population into the new population) is used so that the best members of a population are guaranteed to survive in each generation.

The  $\mu$ -GA differs from a classical GA in that the former uses a very small population (5–10), while the latter uses a larger population with hundreds or even thousands of individuals. Another difference between the  $\mu$ -GA and a classical GA is in the way to maintain diversity. Classical GAs usually use large populations along with mutation operations to achieve diversity upon convergence. In contrast, the  $\mu$ -GA adopts a small population to achieve a relatively fast convergence in the inner loop as compared to a classical GA. The  $\mu$ -GA does not have mutation operations, because diversifying a small population will not give a good representation of the solution space anyway and it will slow down the convergence as well. The diversity of the solutions is achieved by starting with a new, randomly generated population (which is called a "restart" operation in Figure 8) while keeping the best previously obtained solutions (elitism). Note that it is important to keep the best solution from each inner loop convergence to avoid the possibility of extinction of the best members of a population. The global algorithm stops when the prescribed number of generations (200 in this study) is reached (outer loop).

As the  $\mu$ -GA uses binary encoding to represent design variables, along with the range of a design variable, the number of bits to encode the same should also be given as an input. The number of bits needed is determined by the required precision for a design variable.

#### **4.2. Overall $\mu$ -GA based crack identification procedure**

The overall  $\mu$ -GAs-based crack identification procedure is shown in Figure 8 and explained as follows:

4.2.1. Selection of variables and objective/fitness function

The  $\mu$ -GA begins by defining a chromosome, i.e. an array of variables whose values are to be optimised. In our case study, the chromosome has two variables, the crack depth ratio ( $\alpha/H$ ) (the ratio of the crack depth ( $\alpha$ ) to the beam height ( $H$ )) and crack location ratio ( $c/L$ ) (the ratio of the crack location ( $c$ ) to the beam length ( $L$ )). In this study, the crack location is defined by the element number, i.e. cracked element number in the FE mesh and the crack is modelled by inserting the improved 2-D FE into the mesh coinciding with the crack location. Thus, we have:

$$\text{Chromosome} = [\text{Cracked element number, Crack depth ratio}]. \quad (19)$$

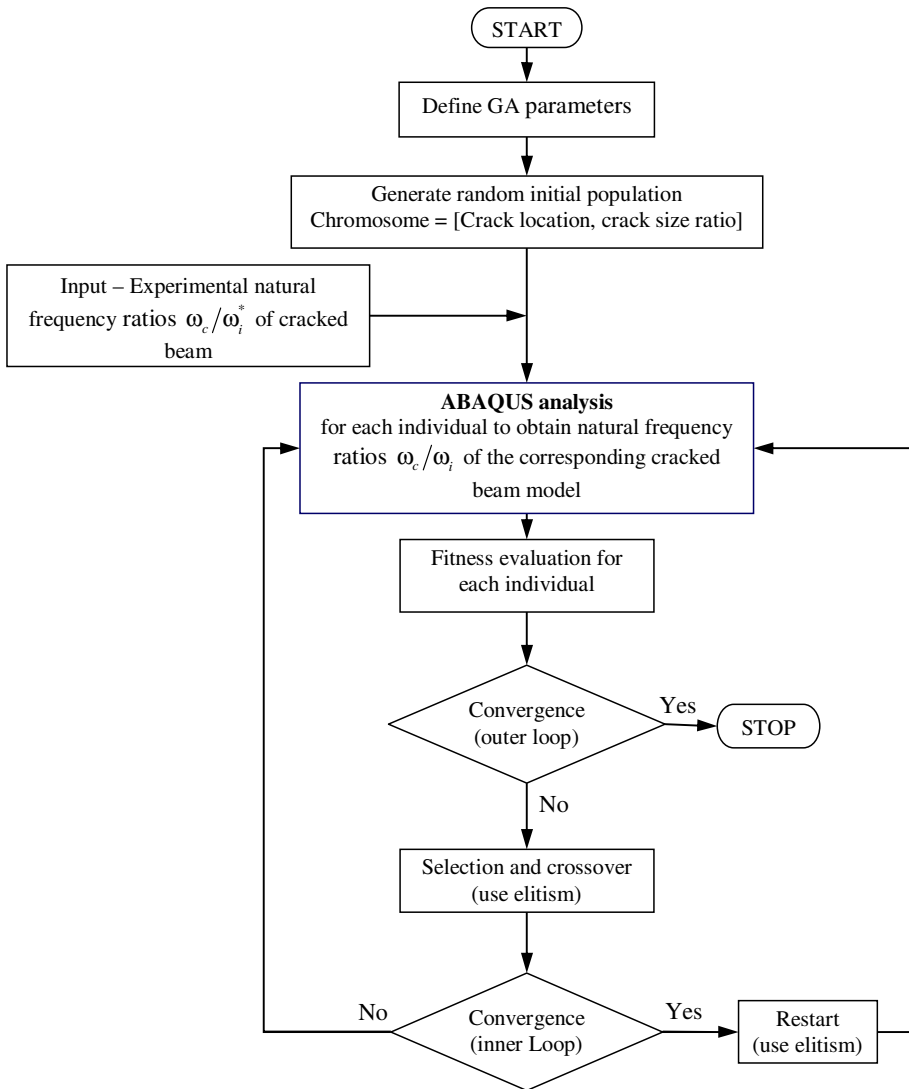


Figure 8. Flowchart of Micro-GA-based crack detection method.

Once a particular chromosome is defined, using the decoded values of the cracked element number and crack depth ratio ( $\alpha/H$ ), the ABAQUS (2004) input file for modal analysis is generated by inserting the improved 2-D FE into the mesh at the location defined by cracked element number. Based on the computed natural frequencies from modal analysis using ABAQUS (2004), the objective/fitness function to be minimised is defined as follows:

$$F(\text{Cracked element number}, \alpha/H) = \sum_{i=1}^n |\omega_c/\omega_i - \omega_c/\omega_i^*|, \quad (20)$$

where  $n$  is the number of frequency ratios being considered,  $\omega_c/\omega_i$  are the natural frequency ratios, which are functions of the cracked element number and crack depth ratio ( $\alpha/H$ ), and are calculated using the improved 2-D FE, and  $\omega_c/\omega_i^*$  are the natural frequency ratios determined through modal analysis experiments, which are applied to the crack detection system as inputs (see Figure 8). An objective/fitness function value of zero indicates an exact match between the values of frequencies.

#### 4.2.2. Chromosome size and encoding

Instead of the standard uniform discretisation of the possible interval of the cracked element number and crack depth ratio ( $\alpha/H$ ), they will be assumed to take one value among a discrete set of values in the possible interval. This is done in order to reduce the search space and also to bias the search away from regions of the search space where they assume unrealistic values.

Crack location and crack depth parameters can be an integer in the range  $1 - 2^n$  and  $1 - 2^m$ , respectively, with  $n$  and  $m$  being the number of bits used to encode each possible value of the cracked element number and crack depth ratio ( $\alpha/H$ ). Crack location and crack depth parameters correspond to an entry in the tables of possible values for the cracked element number and crack depth ratio ( $\alpha/H$ ). The tables are built preserving an ordering of increasing crack location ratio ( $c/L$ ) and crack depth ratio ( $\alpha/H$ ), e.g. integer 1 represents less crack location ratio/crack depth ratio than integer 2 and so on. The tables are built according to a recurrent formula. In this way, one fixes the crack location ratio ( $c/L$ ) and crack depth ratio ( $\alpha/H$ ) for the first integer and the next values are increased as follows:

$$\frac{c}{L}(i) = \frac{c}{L}(i-1) + \Delta\frac{c}{L}, \quad i = 2, \dots, 2^m, \quad (21)$$

$$\frac{\alpha}{H}(i) = \frac{\alpha}{H}(i-1) + \Delta\frac{\alpha}{H}, \quad i = 2, \dots, 2^n, \quad (22)$$

where  $\Delta c/L$  and  $\Delta \alpha/H$  are the increments of crack location ratio ( $c/L$ ) and crack depth ratio ( $\alpha/H$ ), respectively, for each element of the tables. The values of  $\Delta c/L$  and  $\Delta \alpha/H$  are chosen by the user according to the characteristics of the problem at hand, the available prior information (such as the maximum expected level of the crack location ratio ( $c/L$ ) and crack depth ratio ( $\alpha/H$ )), and the values  $n$  and  $m$  adopted. If the exact value of the real crack location ratio ( $c/L$ ) and crack depth ratio ( $\alpha/H$ ) occurring in the structure is not represented in the tables, the  $c/L$  and  $\alpha/H$  should go to the closest value of the respective tables. During the search, if the crack location and crack depth parameter

values falls out of the respective possible entry values in the tables, their values need to be adjusted or reassigned to an entry in the tables corresponding to INT (possible range  $\times$  a uniform random number generated between 0 and 1). An individual chromosome is thus a vector of integers (binary encoded) representing a candidate solution that corresponds to a cracked element number and crack depth ratio ( $\alpha/H$ ).

In practice, the crack identification problem is subject to uncertainties originating in the discrete model as well as in the measurements that are made in the cracked structure. The proposed encoding reduces the search space to be explored, maintains flexibility and allows for the introduction of any available domain knowledge. For instance, one can refine the values in the tables for the cracked element number and crack depth ratio and in any given desired region in the interval of possible values.

#### 4.2.3. *Initial population*

In order to determine the appropriate population size in this study, the various population sizes of 5, 8, 10, 12 and 15 individuals, each represented by a vector generated at random, are tested, in numerical Example 1 presented in the subsequent section. The experience gained in the convergence study of Example 1 is used to analyse the problems presented in other numerical examples.

#### 4.2.4. *Objective/fitness function evaluation*

Natural frequencies are obtained through ABAQUS (2004) modal analysis in conjunction with the improved 2-D FE, and the objective/fitness function is evaluated for each chromosome, decoded values of which represent the cracked element number and crack depth ratio ( $\alpha/H$ ).

#### 4.2.5. *Convergence criterion*

The overall convergence criterion is checked. If the criterion is satisfied, the whole iteration process is stopped; otherwise, it is continued to the next step. In this study, the total prescribed number of generations (= 200) is the overall convergence criterion, and the global algorithm stops when the prescribed number of generations is reached (outer loop).

#### 4.2.6. *Reproduction and iterating the algorithm*

The population for the next generation is obtained through tournament selection and uniform crossover with a crossover rate of 1.0. The elitism strategy is applied to preserve the best members. Inner loop nominal convergence is checked. If the inner loop does not converge, repeat steps (iv) – (vi). Otherwise, restart and regenerate (replacing the discarded chromosomes in the population by new chromosomes) a new population randomly while keeping the best individual from the previous generation. This replacement of the entire population is for searching the overall space for better solutions in  $\mu$ -GA. Repeat steps (iv) – (vi).

### 4.3. ***Reducing computational time required for overall crack identification procedure***

Evaluation of the objective/fitness function for each chromosome in the population using the natural frequencies obtained through ABAQUS (2004) modal analysis, in

conjunction with the improved 2-D FE, is the most computationally intensive operation in the overall  $\mu$ -GA-based crack identification procedure. In the present study, decoded values of the crack depth ratio ( $\alpha/H$ ) and cracked element number along with the objective/fitness function value for each chromosome in the population, is saved. In the global algorithm, after going through the *crossover* operation and *elitism* scheme process, if a particular chromosome remains intact, then the corresponding saved information is used to avoid repetition of the objective/fitness evaluation function using the natural frequencies obtained through ABAQUS (2004) modal analysis, thereby saving the computational time required for the overall  $\mu$ -GA-based crack identification procedure.

## 5. Validation of crack identification technique

The  $\mu$ -GA-based crack detection procedure outlined above in conjunction with the improved 2-D FE is validated both for cases of single crack and multiple cracks in a beam. For single crack detection, validation is performed using the experimental data reported by Silva and Gomes (1990), who performed an extensive set of modal analysis experiments on free-free beams with the goal of providing objective data to validate the proposed techniques for damage detection. For single crack detection, validation is performed using (a) the experimental data reported by Silva and Gomes (1990), who performed an extensive set of modal analysis experiments on free-free beams with the goal of providing objective data to validate the proposed techniques for damage detection; and (b) the experimental data on fixed-fixed and simply supported beams reported by Owolabi, Swamidas, and Seshadri (2003).

The proposed  $\mu$ -GA-based crack detection procedure in conjunction with the improved 2-D FE has the following advantages, which enable its easy extension to the case of beams with multiple cracks: (a) the UEL can be inserted into the FE model at the crack location without any additional mesh refinement in the vicinity of crack, making it possible to model any number of cracks; (b)  $\mu$ -GA avoids some of the weaknesses of conventional gradient-based analytical search methods, including the difficulty in constructing well-defined mathematical models directly from practical inverse problems and is capable of solving an optimisation problem with a large number of variables. While estimating the location and depth of additional cracks in a structure,  $\mu$ -GA just treats them as additional variables.

For multiple cracks detection, validation is performed using (a) the experimental data reported by Patil and Maiti (2005), who tested cantilever beams with two normal-edge cracks of different sizes at different locations starting from the fixed end; and (b) the natural frequencies obtained by FE analysis of uniform beams with two cracks on three pin supports reported by Patil and Maiti (2003). In the numerical results presented below for each test point, the algorithm is run from five different initial random points and it is observed that the answer obtained with different runs converged to the same optimal solution.

### 5.1. Example 1: Single crack in free-free beam

Test specimens adopted by Silva and Gomes (1990) were steel beams with  $.032 \times .016 \text{ m}^2$  rectangular cross-section and .72 m long. The corresponding material properties were:  $E = 2.06 \times 10^{11} \text{ N/m}^2$ ;  $\nu = .29$ ; and  $\rho = 7650 \text{ kg/m}^3$ . In the current study, the same beam is modelled with 89 standard four-node ABAQUS (2004)

elements and one UEL at the location defined by cracked element number. Typical discretisation of free-free beam is shown in Figure 9. Since the beam is edge-cracked, all elements in the top layer are considered to be candidate-cracked elements, even though being a free-free beam top layer or bottom layer is insignificant. Noting that the free-free beam is symmetric with respect to geometry, only half the beam needs to be considered for modal analysis and hence, for the discretisation shown in Figure 9, the possible values of the cracked element number is 23, i.e. the possible value of the cracked element number is between 46 and 68. For the crack depth ratio ( $\alpha/H$ ),  $2^5$  possible values in the interval  $0 < \alpha/H < .5$  with an increment of  $\Delta\alpha/H = .5/32$  are considered. So the cracked element number requires five bits, and the crack depth ratio ( $\alpha/H$ ) requires five bits, and thus every individual chromosome contains 10 bits.

In order to determine the appropriate population size in this study, the various population sizes of 5, 8, 10, 12 and 15 individuals are tested, respectively, for the crack case  $c/L = \alpha/H = .25$  using the proposed  $\mu$ -GA-based crack detection procedure. It can be observed from Figure 10 that all the five population sets show similar convergence rate with different number of generations/computational time. Accordingly, the population size of 10 individuals is selected for the subsequent numerical study. Table 1 presents, for a typical population size of 10 individuals, the decoded values of the cracked element number, crack location ratio ( $c/L$ ), crack depth ratio ( $\alpha/H$ ) and objective/fitness function.

The method for crack identification is verified for several combinations of crack locations and crack sizes listed in Table 2. The first four natural frequencies measured by Silva and Gomes (1990) are used as input in this case. Figures 11 and 12 show the evolution of the objective/fitness function with generations for the crack case  $c/L = \alpha/H = .25$  obtained using  $\mu$ -GA and classical GA, respectively. For the classical GA, the population size is taken as 30, the minimum recommended to prevent genetic drift. For the classical GA, the optimal solution is identified at 34th generation (No. of

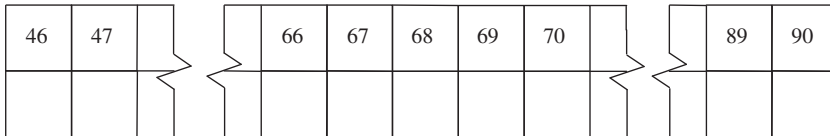


Figure 9. Discretisation of free-free beam with candidate cracked elements in top layer.

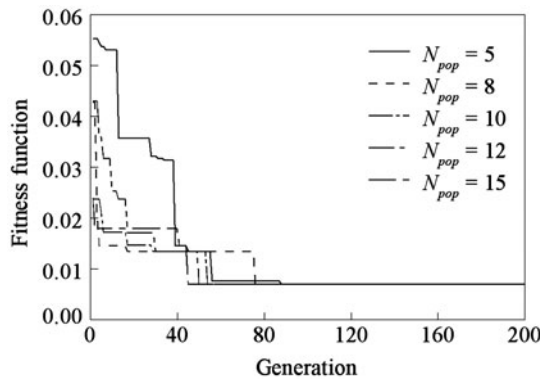


Figure 10.  $\mu$ -GA convergence history (free-free beam).

Table 1. Population of 10 random chromosomes along with the corresponding decoded values and objective/fitness function.

Chromosome	Cracked element no.	Crack		Objective/fitness function
		Location $c/L$	Size $\alpha/H$	
0,001,111,011	49	.0778	.4375	.0861
0,011,100,101	53	.1667	.0938	.0691
0,111,111,001	61	.3444	.4062	.1234
0,110,000,001	58	.2778	.0312	.0695
0,010,010,000	50	.1000	.2656	.077
0,111,011,000	60	.3222	.3906	.0903
0,000,001,110	46	.0111	.2344	.0679
1,000,110,111	63	.3889	.375	.1047
0,011,010,001	52	.1444	.2812	.0827
1,001,111,110	65	.4333	.4844	.1637

Table 2. Comparison of predicted crack positions and sizes of free-free beam with corresponding actual values (example 1).

Crack case	Actual crack (Silva & Gomes, 1990)		Predicted crack		Predicted error (%)	
	Location $c/L$	Size $\alpha/H$	Location $c/L$	Size $\alpha/H$	Location $c/L$	Size $\alpha/H$
1	.125	.125	.144	.078	1.94	4.69
2	.125	.250	.122	.281	.28	3.13
3	.125	.375	.122	.422	.28	4.69
4	.125	.500	.122	.500	.28	.00
5	.250	.125	.233	.094	1.67	3.12
6	.250	.250	.256	.266	.56	1.56
7	.250	.375	.256	.422	.56	4.69
8	.250	.500	.256	.500	.56	.00
9	.375	.125	.433	.078	5.83	4.69
10	.375	.250	.367	.266	.83	1.56
11	.375	.375	.367	.422	.83	4.69
12	.375	.500	.367	.500	.83	.00
13	.500	.125	.500	.109	.00	1.56
14	.500	.250	.500	.297	.00	4.69
15	.500	.375	.500	.422	.00	4.69
16	.500	.500	.500	.500	.00	.00

fitness evaluation required would be  $34 \times 30 = 1020$ ), whereas using  $\mu$ -GA, the optimal solution is identified at 60th generation (No. of fitness evaluation required would be  $60 \times 10 = 600$ ). Typical convergence plots for  $\mu$ -GA for the crack case  $c/L = \alpha/H = .25$  are shown in Figures 13 and 14. From these figures, it can be observed that the damaged site is located at the 22nd generation and the damage extent is correctly evaluated at the 60th generation. The predicted crack location ratio ( $c/L$ ) and crack depth ratio ( $\alpha/H$ ) are .256 and .266, respectively.

Table 2 compares the predicted crack locations and crack sizes with the corresponding actual values. The predicted values are in good agreement with the corresponding actual values. It is worth noting that the average error in the crack location predictions is .90 and the average error in the crack size predictions is 2.73, which is less when compared to the predictions reported by Li, Chen, Ma, and He (2005).

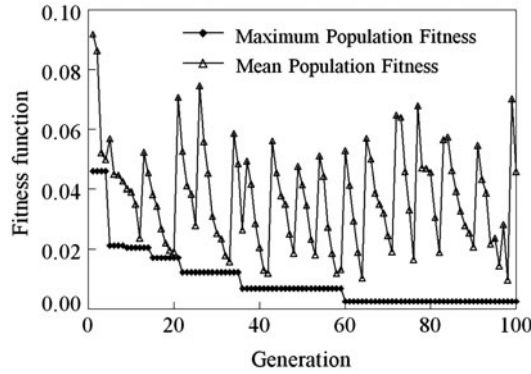


Figure 11. Evolution of mean population fitness and best fitness with generations using  $\mu$ -GA (free-free beam).

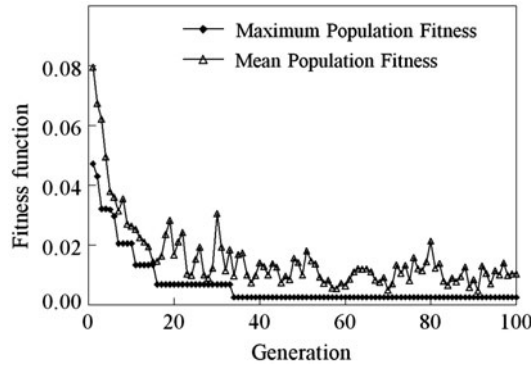


Figure 12. Evolution of mean population fitness and best fitness with generations using classical GA (free-free beam).

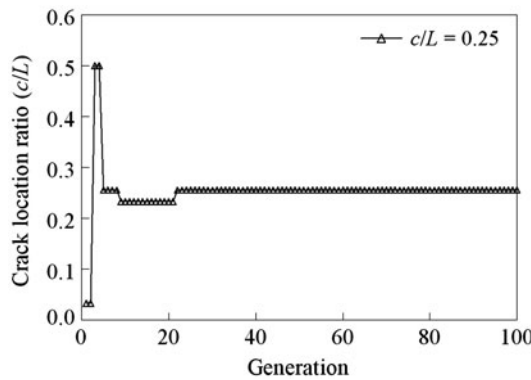


Figure 13. Crack location ratio ( $c/L$ ) as function of generation number (free-free beam).

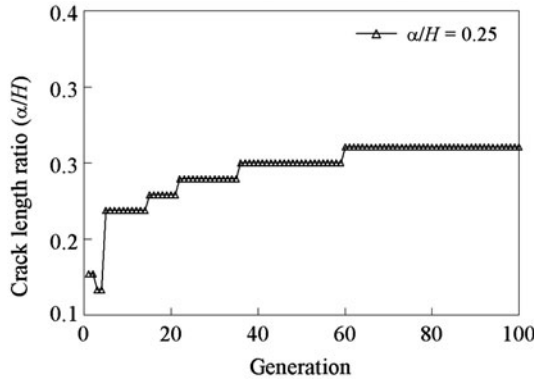


Figure 14. Crack depth ratio ( $\alpha/H$ ) as function of generation number (free-free beam).

**5.2. Example 2: Single crack in simply supported beam**

Owolabi, Swamidas, & Seshadri (2003) tested seven simply supported beam models with cracks at seven different locations, starting from a location nearer to one of the simply supported ends. The crack depth was varied from  $.1H$  to  $.7H$  (the depth of the beam,  $H = .0254m$ ) with an increment of  $.1H$  at each crack location. Each beam model was made of an aluminium bar of cross-sectional area  $.0254 m \times .0254 m$  with a length of  $.650m$ . It had the following material properties: Young’s modulus  $E = 7 \times 10^{10} N/m^2$ , density  $\rho = 2696kg/m^3$  and the Poisson ratio  $\nu = .35$ .

In the current study, the same beam is modelled with 101 standard four-node ABAQUS (2004) elements and one UEL at the top of the beam. Typical discretisation of simply supported beam is shown in Figure 15. Similar to free-free beam, as the simply supported beam is symmetric with respect to geometry, only half the beam needs to be considered for modal analysis and hence, for the discretisation shown in Figure 15, the possible values of the cracked element number is 26, i.e. the possible value of the cracked element number is between 52 and 77. For the crack depth ratio ( $\alpha/H$ ),  $2^5$  possible values in the interval  $0 < \alpha/H < .5$  with an increment of  $\Delta\alpha/H = .5/32$  are considered. So the cracked element number requires five bits, and the crack depth ratio ( $\alpha/H$ ) requires five bits, and thus every individual chromosome contains 10 bits.

Similar to that for free-free beam case, the method for crack identification is verified for several combinations of crack locations and crack sizes listed in Table 3. The first three natural frequencies measured by Owolabi et al. (2003) are used as input in this case. The predicted crack locations and crack sizes are compared with the corresponding actual values in Table 3. The predicted crack locations and crack sizes are in

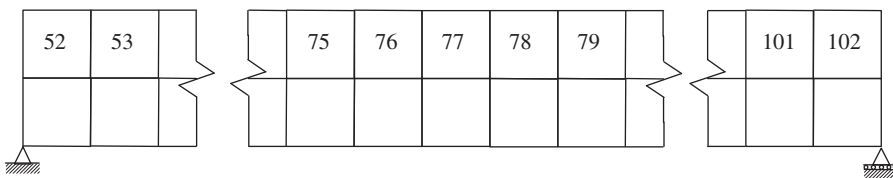


Figure 15. Discretisation of simply supported beam with candidate cracked elements in top layer.

Table 3. Comparison of predicted crack positions and sizes of simply supported beam with corresponding actual values (Example 2).

Crack case	Actual crack (Owolabi et al., 2003)		Predicted crack		Predicted error (%)	
	Location $c/L$	Size $\alpha/H$	Location $c/L$	Size $\alpha/H$	Location $c/L$	Size $\alpha/H$
1	.1875	.10	.2451	.0469	5.76	5.31
2	.1875	.20	.2843	.1562	9.68	4.38
3	.1875	.30	.2255	.2969	3.80	.31
4	.1875	.40	.2451	.4219	5.76	2.19
5	.1875	.50	.2255	.4688	3.80	3.13
6	.3125	.10	.3627	.1094	5.02	.94
7	.3125	.20	.3039	.1562	.86	4.38
8	.3125	.30	.3235	.3125	1.10	1.25
9	.3125	.40	.3235	.4063	1.10	.62
10	.3125	.50	.3039	.4844	.86	1.56
11	.4375	.10	.4216	.0625	1.59	3.75
12	.4375	.20	.4412	.1875	.37	1.25
13	.4375	.30	.4216	.3281	1.59	2.81
14	.4375	.40	.4216	.4219	1.59	2.19
15	.4375	.50	.4216	.5000	1.59	.00
16	.5000	.10	.4216	.0938	7.84	.62
17	.5000	.20	.5000	.1250	.00	7.50
18	.5000	.30	.4412	.3750	5.88	7.50
19	.5000	.40	.4412	.4688	5.88	6.88
20	.5000	.50	.4412	.5000	5.88	.00

good agreement with the actual values with the average error in the crack location and crack size predictions equal to 3.50 and 2.83, respectively.

### 5.3. Example 3: Single crack in fixed-fixed beam

Similar to simply supported beam models, Owolabi et al. (2003) also tested seven fixed-fixed beam models having the same geometrical and material properties with cracks at seven different locations, starting from a location nearer to one of the clamped end. In the current study, the fixed-fixed beam is modelled with the same discretisation as shown in Figure 15 (except that the support ends are fixed-fixed, instead of simply supported), and hence every individual chromosome contains 10 bits.

Similar to that for simply supported beam case, using the first three natural frequencies measured by Owolabi et al. (2003) are used as input, the method for crack identification is verified for several combinations of crack locations and crack sizes listed in Table 4. The comparison of the predicted crack locations and crack sizes with the corresponding actual values in Table 4 shows that the predicted values are in good agreement with the actual values. The average error in the crack location predictions is 2.46 and the average error in the crack size predictions is 2.63.

### 5.4. Example 4: Two cracks in cantilever beam

Patil and Maiti (2005) tested cantilever beams with two normal edge cracks of different sizes at different locations, starting from the fixed end. The crack depth was varied from  $.1H$  to  $.65H$  (the depth of the beam,  $H = .0191$  m). Each beam model was made of an

Table 4. Comparison of predicted crack positions and sizes of fixed-fixed beam with corresponding actual values (Example 3).

Crack case	Actual crack (Owolabi et al., 2003)		Predicted crack		Predicted error (%)	
	Location $c/L$	Size $\alpha/H$	Location $c/L$	Size $\alpha/H$	Location $c/L$	Size $\alpha/H$
1	.1875	.10	.2843	.0469	9.68	5.31
2	.1875	.20	.2255	.1562	3.80	4.38
3	.1875	.30	.2451	.2344	5.76	6.56
4	.1875	.40	.2059	.3906	1.84	.94
5	.1875	.50	.2451	.4531	5.76	4.69
6	.3125	.10	.3039	.0469	.86	5.31
7	.3125	.20	.3039	.1562	.86	4.38
8	.3125	.30	.3039	.2813	.86	1.88
9	.3125	.40	.3235	.3906	1.10	.94
10	.3125	.50	.3235	.4844	1.10	1.56
11	.4375	.10	.4608	.1094	2.33	.94
12	.4375	.20	.4608	.2188	2.33	1.88
13	.4375	.30	.4412	.3438	.37	4.38
14	.4375	.40	.4412	.4063	.37	.62
15	.4375	.50	.4412	.5000	.37	.00
16	.5000	.10	.5000	.1094	.00	.94
17	.5000	.20	.5000	.1875	.00	1.25
18	.5000	.30	.4608	.3438	3.92	4.38
19	.5000	.40	.4804	.4219	1.96	2.19
20	.5000	.50	.4412	.5000	5.88	.00

aluminium alloy bar of cross-sectional area  $.0191 \text{ m} \times .0064 \text{ m}$  with a length of  $.24 \text{ m}$ . It had the following material properties: Young’s modulus  $E = 70.06 \times 10^9 \text{ N/m}^2$ , density  $\rho = 2645.19 \text{ kg/m}^3$  and the Poisson ratio  $\nu = .35$ .

In the current study, the cantilever beam with two normal edge cracks is modelled with 50 standard four node elements ABAQUS (2004) elements and two UELs at the top of the beam. For the typical discretisation of cantilever beam shown in Figure 16, the possible values of the cracked element number are 26, i.e. the possible value of the cracked element number is between 27 and 52. For the crack depth ratio ( $\alpha/H$ ),  $2^5$  possible values in the interval  $0 < \alpha/H < .5$  with an increment of  $\Delta\alpha/H = .5/32$  are considered. So the cracked element number requires five bits, and the crack depth ratio ( $\alpha/H$ ) requires five bits, and thus every individual chromosome for cantilever beam with two normal edge cracks contains  $2 \times 10 = 20$  bits.

Figure 17 shows the evolution of the objective/fitness function with generations for the crack case  $c_1/L = .100$ ,  $c_2/L = .496$  and  $\alpha_1/H = \alpha_2/H = .450$  obtained using  $\mu$ -GA. The optimal solution is identified at 102th generation. Typical convergence plots

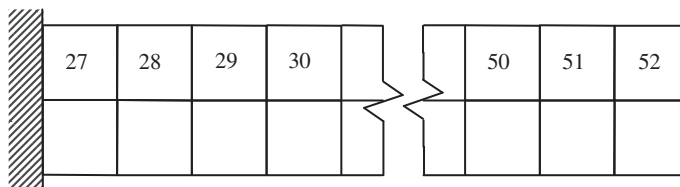


Figure 16. Discretisation of cantilever beam with candidate cracked elements in top layer (cantilever beam).

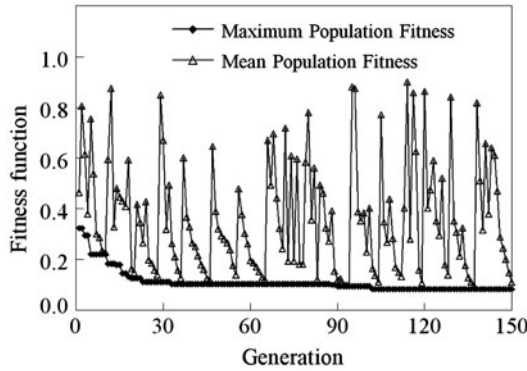


Figure 17. Evolution of mean population fitness and best fitness with generations using  $\mu$ -GA (cantilever beam).

for the same crack case are shown in Figures 18 and 19 and it can be seen that the damaged sites are located at the 23rd and 102nd generations and the damage extents are correctly evaluated at the 90th and 88th generations. The predicted crack location ratio ( $c/L$ ) and crack depth ratio ( $\alpha/H$ ) are (.135, .481), and (.469, .469), respectively.

Similar to that for single crack beam cases, the method for crack identification is verified for several combinations of crack locations and crack sizes listed in Table 5. The first five natural frequencies measured by Patil and Maiti (2005) are used as input in this case. The predicted crack locations and crack sizes are compared with the corresponding actual values in Table 5. The predicted crack locations and crack sizes are in good agreement with the actual values with the average error in the crack location and crack size predictions equal to 3.01 and 5.04, respectively.

**5.5. Example 5: two cracks in uniform beams on three-pin supports**

Patil and Maiti (2003) reported natural frequencies obtained by FE analysis of uniform beams with two cracks on three-pin supports, starting from one of the simply supported ends. The crack depth was varied from  $.1H$  to  $.5H$  (the depth of the beam,  $H = .02$  m). Uniform beam on three-pin supports model was made of cross-sectional area  $.02m \times .012$  m with a length of each span  $.3m$ . It had the following material

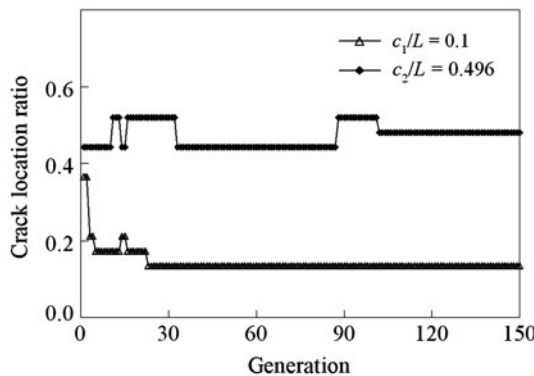


Figure 18. Crack location ratios ( $c/L$ ) as function of generation number (cantilever beam).

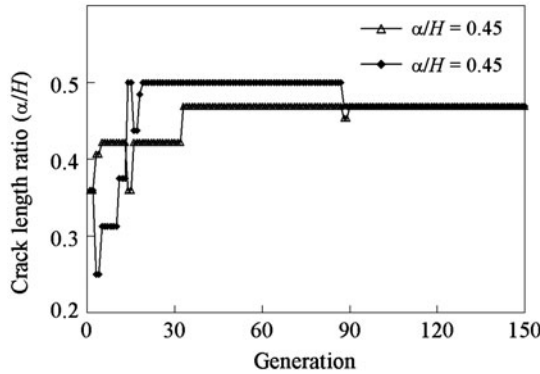


Figure 19. Crack depth ratios ( $\alpha/H$ ) as function of generation number (cantilever beam).

Table 5. Comparison of predicted crack positions and sizes of cantilever beam with corresponding actual values (Example 4).

Crack case	Actual crack (Patil & Maiti, 2005)		Predicted crack		Predicted error (%)		
	Location $c/L$	Size $\alpha/H$	Location $c/L$	Size $\alpha/H$	Location $c/L$	Size $\alpha/H$	
1	Crack 1	.200	.200	.188	1.15	1.25	
	Crack 2	.498	.430	.481	.500	1.72	7.00
2	Crack 1	.250	.455	.212	.453	3.85	.19
	Crack 2	.500	.250	.481	.359	1.92	1.94
3	Crack 1	.100	.450	.135	.469	3.46	1.88
	Crack 2	.496	.450	.481	.469	1.52	1.88
4	Crack 1	.250	.460	.212	.438	3.85	2.25
	Crack 2	.500	.150	.442	.313	5.77	16.25
5	Crack 1	.150	.300	.173	.313	2.31	1.25
	Crack 2	.496	.455	.481	.500	1.52	4.50
6	Crack 1	.250	.434	.212	.391	3.85	4.34
	Crack 2	.500	.350	.442	.406	5.77	5.63
7	Crack 1	.250	.420	.212	.359	3.85	6.06
	Crack 2	.500	.400	.442	.438	5.77	3.75
8	Crack 1	.250	.150	.250	.234	.00	8.44
	Crack 2	.500	.450	.519	.500	1.92	5.00

properties: Young’s modulus  $E = 210 \times 10^9 \text{ N/m}^2$ , density  $\rho = 7860 \text{ kg/m}^3$  and the Poisson ratio  $\nu = .3$ .

Each span of the uniform beam is modelled with 59 standard four-node ABAQUS (2004) elements and one UEL at the top of the beam. Typical discretisation of uniform beam is shown in Figure 20. For the discretisation shown in Figure 20, the possible values of the cracked element number are 60, i.e. considering one crack in each span the possible value of the cracked element number for the first and second crack is between 61–90 and 91–120, respectively. For the crack depth ratio ( $\alpha/H$ ),  $2^5$  possible values in the interval  $0 < \alpha/H < .5$  with an increment of  $\Delta\alpha/H = .5/32$  are considered. So the cracked element number requires five bits, and the crack depth ratio ( $\alpha/H$ ) requires five bits, and thus every individual chromosome for uniform beam with two normal-edge cracks contains  $2 \times 10 = 20$  bits.

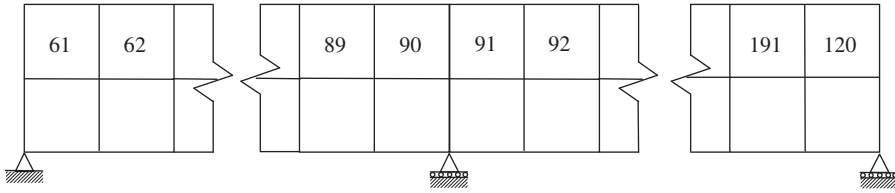


Figure 20. Discretisation of uniform beam with candidate cracked elements in top layer.

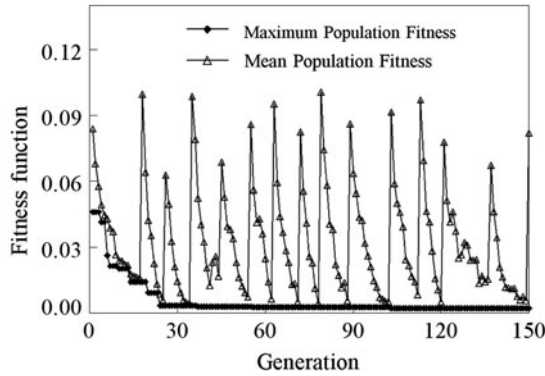


Figure 21. Evolution of mean population fitness and best fitness with generations using  $\mu$ -GA (uniform beam).

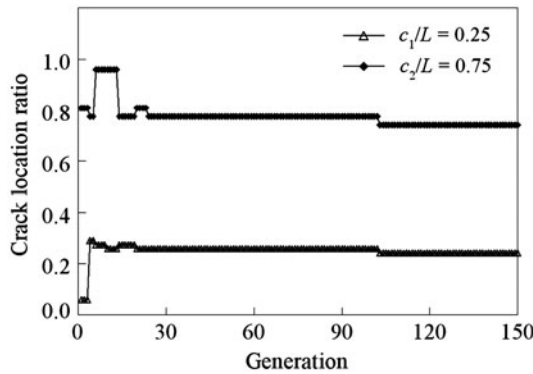


Figure 22. Crack location ratios ( $c/L$ ) as function of generation number (uniform beam).

Figure 21 shows the evolution of the objective/fitness function with generations for the crack case  $c_1/L = .250$ ,  $c_2/L = .750$  and  $\alpha_1/H = .250$ ,  $\alpha_2/H = .150$  obtained using  $\mu$ -GA. The optimal solution is identified at 103rd generation. Typical convergence plots for the same crack case are shown in Figures 22 and 23 and it can be seen that the damaged sites and the damage extents are correctly evaluated at the 103rd generation. The predicted crack location ratio ( $c/L$ ) and crack depth ratio ( $\alpha/H$ ) are (.242, .742) and (.266, .141), respectively.

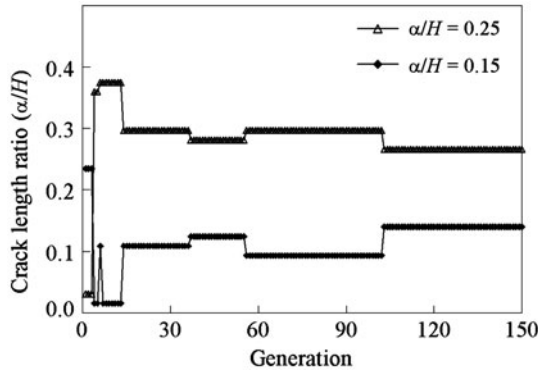


Figure 23. Crack depth ratios ( $\alpha/H$ ) as function of generation number (uniform beam).

Table 6. Comparison of predicted crack positions and sizes of uniform beam with corresponding actual values (Example 5).

Crack case	Actual crack (Patil & Maiti, 2003)		Predicted crack		Predicted error (%)	
	Location $c/L$	Size $\alpha/H$	Location $c/L$	Size $\alpha/H$	Location $c/L$	Size $\alpha/H$
1 Crack 1	.250	.250	.242	.266	.83	1.56
	.750	.150	.742	.141	.83	.94
2 Crack 1	.250	.250	.258	.281	.83	3.13
	Crack 2	.750	.250	.758	.266	.83
3 Crack 1	.250	.250	.258	.188	.83	6.25
	Crack 2	.750	.350	.758	.422	.83
4 Crack 1	.250	.250	.258	.328	.83	7.81
	Crack 2	.750	.500	.758	.500	.83
5 Crack 1	.300	.150	.325	.141	2.50	.94
	Crack 2	.600	.250	.592	.266	.83
6 Crack 1	.350	.250	.358	.203	.83	4.69
	Crack 2	.600	.300	.608	.375	.83
7 Crack 1	.400	.350	.392	.406	.83	5.63
	Crack 2	.700	.350	.708	.375	.83
8 Crack 1	.450	.150	.475	.094	2.50	5.63
	Crack 2	.650	.150	.625	.156	2.50

Similar to that for single crack beam cases, the method for crack identification is verified for several combinations of crack locations and crack sizes listed in Table 6. The first five natural frequencies reported by Patil and Maiti (2003) are used as input in this case. The predicted crack locations and crack sizes are compared with the corresponding actual values in Table 6. The predicted crack locations and crack sizes are in good agreement with the actual values with the average error in the crack location and crack size predictions equal to 1.15 and 3.59, respectively.

**6. Conclusions**

This paper presents an improved 2-D FE with an embedded edge crack for crack depth ratios ranging up to .9 and for predicting natural frequency of a cracked beam more

accurately. The FRANC2DL FE code is used with the  $J$ -integral option to extract the stress intensity factors from stress–strain fields around the crack tip location. The geometric factors for various loading cases of the cracked element for crack depth ratios ranging up to .9 are obtained by means of curve-fitting techniques, and they are subsequently used to obtain the components of the stiffness matrix for the cracked element from the Castigliano's first theorem using fracture mechanics concepts. The element is implemented in the commercial FE code ABAQUS as UEL subroutine. The first natural frequency for the bending mode for several beam cases with different damage locations, obtained using the proposed improved FE, are in good agreement with the available experimental data.  $\mu$ -GA-based crack identification methodology to detect crack location and size in conjunction with the improved cracked element is also presented for singularity problems like a cracked beam. The proposed  $\mu$ -GA-based crack detection procedure using the improved 2-D FE is validated using the available experimental and FE modal analysis data reported in the existing literature. The predicted crack locations and crack sizes are in good agreement with the actual values. Future work will attempt to extend this approach to account for the influence of the plastic zone ahead of the crack tip on the flexibility of structures.

### Acknowledgement

The first author would like to acknowledge the fellowship of the Tata Consultancy Services during course of this research.

### References

- ABAQUS. (2004). Documentation (Version 6.5). Pawtucket, RI: Hibbit, Karlson & Sorensen.
- Amstutz, S., Horchani, I., & Masmoudi, M. (2005). Crack detection by the topological gradient method. *Control and Cybernetics*, *34*, 81–101.
- Cakoni, F., & Colton, D. (2003). The linear sampling method for cracks. *Inverse Problems*, *19*, 279–295.
- Carroll, D. L. (1996). Genetic algorithms and optimizing chemical oxygen-iodine lasers. In H. Wilson, R. Batra, C. Bert, A. Davis, R. Schapery, D. Stewart, & F. Swinson (Eds.), *Developments in theoretical and applied mechanics* (Vol. XVIII, pp. 411–424). Tuscaloosa, Alabama, USA: School of Engineering, The University of Alabama.
- Chaudhari, T. D., & Maiti, S. K. (2000). A study of vibration of geometrically segmented beams with and without crack. *International Journal of Solids and Structures*, *37*, 761–779.
- Chinchalkar, S. (2001). Determination of crack location in beams using natural frequencies. *Journal of Sound and Vibration*, *247*, 417–429.
- Chondros, T. G., Dimarogonas, A. D., & Yao, J. (1998). A continuous cracked beam vibration theory. *Journal of Sound and Vibration*, *215*, 17–34.
- Chondros, T. G., Dimarogonas, A. D., & Yao, J. (2001). Vibration of a beam with a breathing crack. *Journal of Sound and Vibration*, *239*, 57–67.
- Chou, J. H., & Ghaboussi, J. (2001). Genetic algorithm in structural damage detection. *Computers and Structures*, *79*, 1335–1353.
- Dado, M. H. (1997). A comprehensive crack identification algorithm for beam under different end conditions. *Applied Mechanics*, *51*, 381–398.
- Doebling, S. W., Farrar, C. R., Prime, M. B., & Shevitz, D. W. (1996). *Damage identification and health monitoring of structural and mechanical systems from changes in their vibration characteristics: A literature review*, (Technical, Report LA13070MS). Los Alamos, NM: Los Alamos National Laboratory.
- Friswell, M. I., Penny, J. E. T., & Garvey, S. D. (1998). A combined genetic and eigensensitivity algorithm for the location of damage in structures. *Computers and Structures*, *69*, 547–556.
- Garreau, S., Guillaume, P., & Masmoudi, M. (2000). The topological asymptotic for PDE systems: The elasticity case. *SIAM Journal on Control and Optimization*, *39*, 1756–1778.

- Gawronski, W., & Sawicki, J. T. (2000). Structural damage detection using modal norms. *Journal of Sound and Vibration*, 229, 194–198.
- Goldberg, D. E. (1989). *Genetic algorithms in search, optimization, and machine learning*. Reading, MA: Addison-Wesley.
- Goldberg, D. E. (1989). Sizing populations for serial and parallel genetic algorithms. In *Proceeding 3rd International Conference on Genetic Algorithms and Their Applications* (pp. 70–79). Fairfax, Virginia, USA: George Mason University.
- Gondhalekar, S. (1992). *Development of a software tool for crack propagation analysis in two dimensional layered structures* (MS thesis). Kansas State University.
- Gounaris, G. D., Papadopoulos, C. A., & Dimarogonas, A. D. (1996). Crack identification in beams by coupled response measurements. *Computers and Structures*, 58, 299–305.
- Harrison, C., & Butler, R. (2001). Locating delaminations in composite beams using gradient techniques and a genetic algorithm. *American Institute of Aeronautics and Astronautics Journal*, 39, 1383–1389.
- Haupt, R. L., & Haupt, S. E. (2004). *Practical genetic algorithms* (2nd ed.). Hoboken, New Jersey: John Wiley & Sons, Inc.
- Hu, N., Wang, X., Fukunaga, H., Yao, Z. H., Zhang, H. X., & Wu, Z. S. (2001). Damage assessment of structures using modal test data. *International Journal of Solids and Structures*, 38, 3111–3126.
- James, M. A., & Swenson, D. V. (1999). A software framework for two dimensional mixed mode-I/II elastic-plastic fracture. In K. J. Miller & D. L. McDowell (Eds.), *Mixed-mode crack behavior*, ASTM STP 1359 (pp. 111–126). West Conshohocken, PA: American Society for Testing and Materials.
- Kosmatka, J. B., & Ricles, J. M. (1999). Damage detection in structures by modal vibration characterization. *Journal of Structural Engineering*, 125, 1384–1392.
- Krawczuk, M. (2002). Application of spectral beam finite element with a crack iterative search technique for damage detection. *Finite Elements in Analysis and Design*, 38, 537–548.
- Krawczuk, M., Palacz, M., & Ostachowicz, W. (2003). The dynamic analysis of a cracked Timoshenko beam by the spectral element method. *Journal of Sound and Vibration*, 264, 1139–1153.
- Krishnakumar, K. (1989). Micro-genetic algorithms for stationary and nonstationary function optimization. *SPIE, Intelligent Control and Adaptive Systems*, 1196, 282–296.
- Law, S. S., Chan, T. H., & Wu, D. (2001). Efficient numerical modal for the damage detection of large scale structure. *Engineering Structures*, 23, 436–451.
- Lee, J. (2009). Identification of multiple cracks in a beam using vibration amplitudes. *Journal of Sound and Vibration*, 3206, 205–212.
- Lee, J., Kim, S.-M., Park, H.-S., & Woo, B.-H. (2005). Optimum design of cold-formed steel channel beams using micro genetic algorithm. *Computers and Structures*, 27, 17–24.
- Lele, S. P., & Maiti, S. K. (2002). Modelling of transverse vibration of short beams for crack detection and measurement of crack extension. *Journal of Sound and Vibration*, 257, 559–583.
- Li, B., Chen, X., Ma, J., & He, Z. (2005). Detection of crack location and size in structures using wavelet finite element methods. *Journal of Sound and Vibration*, 285, 767–782.
- Liang, R. Y., Choy, F. K., & Hu, J. (1991). Detection of cracks in beam structures using measurements of natural frequencies. *Journal of the Franklin Institute*, 328, 505–518.
- Liang, R. Y., & Hu, J. (1993). An integrated approach to detection of cracks using vibration characteristics. *Journal of the Franklin Institute*, 330, 841–853.
- Mahmoud, M. A., Abu Zaid, M., & Al Harashani, S. (1999). Numerical frequency analysis of uniform beams with a transverse crack. *Communications in Numerical Methods in Engineering*, 15, 709–715.
- Mares, C., & Surace, C. (1996). An application of genetic algorithms to identify damage in elastic structures. *Journal of Sound and Vibration*, 195, 195–215.
- Messina, A., Williams, E. J., & Contursi, T. (1998). Structural damage detection by a sensitivity and statistical-based method. *Journal of Sound and Vibration*, 216, 791–808.
- Mitchell, M. (1996). *An introduction to genetic algorithms*. Cambridge, Massachusetts, USA: MIT Press.

- Montalvao, D., Maia, N. M. M., & Ribeiro, A. M. R. (2006). A review of vibration-based structural health monitoring with special emphasis on composite materials. *The Shock and Vibration Digest*, 38, 295–324.
- Morassi, A. (2001). Identification of a crack in a rod based on changes in a pair of natural frequencies. *Journal of Sound and Vibration*, 242, 577–596.
- Nandwana, B. P., & Maiti, S. K. (1997a). Detection of the location and size of a crack in stepped cantilever beams based on measurements of natural frequencies. *Journal of Sound and Vibration*, 203, 435–446.
- Nandwana, B. P., & Maiti, S. K. (1997b). Modelling of vibration of beam in presence of inclined edge or internal crack for its possible detection based on frequency measurements. *Engineering Fracture Mechanics*, 58, 193–205.
- Narkis, Y. (1994). Identification of crack location in vibrating simply supported beams. *Journal of Sound and Vibration*, 172, 549–558.
- Nikolakopoulos, P. G., Katsareas, D. E., & Papadopoulos, C. A. (1997). Crack identification in frame structures. *Computers and Structures*, 64, 389–406.
- Osyczka, A., & Kundu, S. (1996). A modified distance method for multicriteria optimization, using genetic algorithms. *Computers & Industrial Engineering*, 30, 871–882.
- Owolabi, G., Swamidass, A., & Seshadri, R. (2003). Crack detection in beams using changes in frequencies and amplitudes of frequency response functions. *Journal of Sound and Vibration*, 265, 1–22.
- Papadopoulos, C. A., & Dimarogonas, A. D. (1987). Coupled longitudinal and bending vibrations of a rotating shaft with an open crack. *Journal of Sound and Vibration*, 117, 81–93.
- Patil, D. P., & Maiti, S. K. (2003). Detection of multiple cracks using frequency measurements. *Engineering Fracture Mechanics*, 70, 1553–1572.
- Patil, D. P., & Maiti, S. K. (2005). Experimental verification of a method of detection of multiple cracks in beams based on frequency measurements. *Journal of Sound and Vibration*, 281, 439–451.
- Peimani, M., Vakil-Baghmisheh, M. T., Sadeghi, M., & Etefagh, M. M. (2005). Locating damage in beam like structures with neural networks. In *Proceedings of Intelligent Systems, CIS2005*, Tehran, p. 54.
- Pezeshk, S., Camp, C. V., & Chen, D. (2000). Design of nonlinear framed structures using genetic optimization. *Journal of Structural Engineering*, 126, 382–388.
- Potimiche, G. P., Hearndon, J., Daniewicz, S. R., Parker, D., Cuevas, P., Wang, P. T., & Horstemeyer, M. F. (2008). A two-dimensional damaged finite element for fracture applications. *Engineering Fracture Mechanics*, 75, 3895–3908.
- Ratcliffe, C. P. (2000). Frequency and curvature based experimental method for locating damage in structures. *Journal of Vibration and Acoustics*, 122, 324–329.
- Rus, G., Lee, S. Y., Chang, S. Y., & Wooh, S. C. (2006). Optimized damage detection of steel plates from noisy impact test. *International Journal for Numerical Methods in Engineering*, 68, 707–727.
- Rus, G., Lee, S. Y., & Gallego, R. (2005). Defect identification in laminated composite structures by BEM from incomplete static data. *International Journal of Solids and Structures*, 42, 1743–1758.
- Sahin, M., & Sheno, R. A. (2003). Quantification and localization of damage in beam-like structures by using artificial neural networks with experimental validation. *Engineering Structures*, 25, 1785–1802.
- Sahoo, B., & Maity, D. (2007). Damage assessment of structures using hybrid neurogenetic algorithm. *Applied Soft Computing*, 7, 89–104.
- Salawu, O. S. (1997). Detection of structural damage through changes in frequency: A review. *Engineering Structures*, 19, 718–723.
- Shifrin, E. I., & Ruotolo, R. (1999). Natural frequencies of a beam with an arbitrary number of cracks. *Journal of Sound and Vibration*, 222, 409–423.
- Silva, J. M., & Gomes, A. J. L. (1990). Experimental dynamic analysis of cracked free-free beams. *Experimental Mechanics*, 30, 20–25.
- Sohn, H., Farrar, C., Hemez, F., Shunk, D., Stinemates, D., & Nadler, B. (2003). *A review of structural health monitoring literature: 1996–2001* (Technical, Report LA13976MS). Los Alamos, NM: Los Alamos National Laboratory.

- Tada, H., Paris, P. C., & Irwin, G. R. (2000). *The stress analysis of cracks handbook* (3rd ed.). New York, NY: ASME Press.
- Vestroni, F., & Capecchi, D. (2000). Damage detection in beam structures based on frequency measurements. *Journal of Engineering Mechanics*, 126, 761–768.
- Wawrzynek, P. A., and Ingraffea, A. R. (1994). *FRANC2D: Two-dimensional crack propagation simulator, Version 2.7 User's Guide*, NASA CR 4572.
- Wawrzynek, P. A., & Ingraffea, A. R. (1987). Interactive finite element analysis of fracture processes: An integrated approach. *Theoretical and Applied Fracture Mechanics*, 8, 137–150.
- Wendtland, D. (1972). *Änderung der biegegegenfrequenzen einer idealisierten Schaufel durch Risse* (PhD Dissertation). University of Karlsruhe.
- Xia, Y., and Hao, H. (2001). A genetic algorithm for structural damage detection based on vibration data. In *Proceedings of 19th International Modal Analysis Conferences*. Kissimmee, FL, pp. 1381–1387.